Inhibiting Phase Transfer of Protein Nanoparticles by Surface Camouflage-A Versatile and Efficient Protein Encapsulation Strategy

Zhang, Pei

2021-11-24

Zhang , P , Li , C , Huang , T , Bai , Y , Quan , P , Li , W , Zhang , Z , Zhang , F , Liu , Z , Wan , B , Correia , A , Zhang , J , Wu , X , Hirvonen , J T , Santos , H A , Fan , J , Cai , T & Liu , D 2021 , ' Inhibiting Phase Transfer of Protein Nanoparticles by Surface Camouflage-A Versatile and Efficient Protein Encapsulation Strategy ' , Nano Letters , vol. 21 , no. 22 , pp. 9458-9467 . https://doi.org/10.1021/acs.nanolett.1c02438

http://hdl.handle.net/10138/351886
https://doi.org/10.1021/acs.nanolett.1c02438

unspecified
acceptedVersion

Inhibiting phase transfer of protein nanoparticles by surface camouflage--A versatile and efficient protein encapsulation strategy

Pei Zhang[1, 2], *Cong Li*[3], *Tianhe Huang*[2], *Yuancheng Bai*[2], *Peng Quan*[4], *Wei Li*[1], *Zifan Zhang*[2], *Feng Zhang*[1], *Zehua Liu*[1], *Bowen Wan*[3], *Alexandra Correia*[1], *Jie Zhang*[2], *Xuri Wu*[5], *Jouni T. Hirvonen*[1], *Hélder A. Santos*[1, 6], *Jin Fan*[3], *Ting Cai*[2] *and Dongfei Liu*[2, 1*]

[1]Drug Research Program, Division of Pharmaceutical Chemistry and Technology, Faculty of Pharmacy, University of Helsinki, Helsinki 00014, Finland

[2]State Key Laboratory of Natural Medicines, Department of Pharmaceutical Science, China Pharmaceutical University, Nanjing 210009, China
E-mail: dongfei.liu@cpu.edu.cn

[3]Department of Orthopaedics, The First Affiliated Hospital of Nanjing Medical University, Nanjing 210029, China

[4]Department of Pharmaceutical Science, School of Pharmacy, Shenyang Pharmaceutical University, Shenyang 110016, China

[5]State Key Laboratory of Natural Medicines and Laboratory of Chemical Biology, China Pharmaceutical University, Nanjing 210009, China

[6]Helsinki Institute of Life Science (HiLIFE), University of Helsinki, Helsinki 00014, Finland

Key words: phase transfer inhibition, surface camouflage, high drug loading, controlled release, protein encapsulation

Abstract

Engineering a system with high mass fraction of active ingredients, especially water-soluble proteins, is still an ongoing challenge. In this work, we developed a versatile surface camouflage strategy that can engineer systems with ultrahigh mass fraction of proteins. By formulating protein molecules into nanoparticles, the demand of molecular modification was transformed into surface camouflage of protein nanoparticles. Thanks to electrostatic attractions and van der Waals interactions, we camouflaged the surface of protein nanoparticles through the adsorption of carrier materials. The adsorption of carrier materials successfully inhibited the phase transfer of insulin, albumin, β-lactoglobulin and ovalbumin nanoparticles. As a result, the obtained microcomposites featured with a record of protein encapsulation efficiencies nearly 100%, and a record of protein mass fraction of 77%. After encapsulation in microcomposites, the insulin revealed hypoglycemic effect for at least 14 days with one single injection, while that of insulin solution was only 4 h.

Encapsulation is a powerful technique to embed active ingredients into another inert material [1-3], such as water-insoluble polymers [4, 5] and phospholipids [6]. The physical barrier formed by inert materials controls the release of incorporated active ingredients [7-9] and, consequently, improves many properties of these ingredients. For example, the encapsulation with an epoxy resin reduces the lead leakage from damaged lead halide perovskite solar modules [10]. Microspheres extend the apparent half-life of encapsulated therapeutics and eliminate the need for multiple doses [11]. Regarding water-soluble active ingredients, like proteins and peptides, it is a challenge to dissolve them together with the inert material in the same phase [12-14]. A variety of approaches, such as forming hexamers [15] and bonding with inert materials [16], have been developed to address the miscibility issue between active ingredients and carrier materials. However, these approaches demand molecular features for both active ingredients and carrier molecules. A versatile strategy, regardless of the types of active ingredients, that can engineer systems with high mass fraction of water-soluble ingredients is highly desirable.

To enable the efficient encapsulation of active ingredients, we proposed a surface camouflage strategy (**Figure 1**a). In this strategy, active ingredients were formulated into nanoparticles, and the camouflage by carrier materials was only demanded at the surface of active ingredient nanoparticles. After surface camouflage, every water-soluble active ingredient nanoparticle was surrounded by a layer of carrier material molecules. This surface camouflage was anticipated to improve the disperstiveness of active ingredient nanoparticles in the oil phase together with the materials and therefore, rending the miscibility issue between active ingredients and carrier materials. After the solidification of engineered oil droplets, this adsorbed layer was supposed to efficiently prolong the release of water-soluble ingredients. As electrostatic attraction usually plays a dominant role among surface interactions [17-19], a cationic polymer with abundant amino groups, spermine-modified acetylated dextran (ADS), served as

the carrier material (**Figure 1**b)[20]. Acetylated dextran (AD), a polymer without amino groups, was chosen as the control material.

At first, we studied the interaction between protein nanoparticles and polymer molecules in the oil phase. Insulin was selected as the model active ingredient, for which the improvement of *in vivo* half-life is urgently needed to reduce its administration frequency [21]. The amount of carrier materials adsorbed onto the surface of insulin nanoparticles was quantified using a quartz crystal microbalance. The quartz disc was coated with insulin nanoparticles by a two-step spinning (800 rpm, 15 s; 4000, 30 s) with a surface coverage of 85.2% (**Figure S1**). When ADS dimethyl carbonate solution (10 mg/mL) flew over the surface of a quartz disc coated with insulin nanoparticles, the oscillation frequency of the third overtone decreased for approximately 49.8 Hz (**Figure 1**c). The adsorbed mass of ADS and dimethyl carbonate on the insulin nanoparticle-coated disc was 751.9 ± 105.8 ng/cm^2 (**Figure 1**d), which was significantly ($P < 0.01$) higher than that of AD solution (191.6 ± 109.9 ng/cm^2).

The isothermal titration calorimetry was used to elucidate the thermodynamic profile of the interaction between polymer molecules and insulin nanoparticles. Between two adjacent injections of polymer into insulin suspension (**Figure 1**e), an equilibrium of free and adsorbed polymer established, and heat was released (exothermic). Surface adsorption of AD and ADS onto insulin nanoparticles was both driven by enthalpically favorable changes (**Figure 1**f). The enthalpy change (ΔH) is an indicator that reflects the interaction strength between nanoparticles and adsorbed agents [22, 23]. For insulin nanoparticles, the interaction strength (in term of ΔH) with ADS (-257.1 ± 28.0 kJ/mol) was stronger than that with AD (-29.5 ± 0.7 kJ/mol). As shown in **Figure 1**g, the value of unfavorable entropy loss ($\Delta S < 0$) for ADS (-756.2 ± 54.9 J/mol·K) was much higher than that for AD (-10.5 ± 2.5 J/mol·K), which could be ascribed to the solvation of nanoparticles after ADS adsorption [24]. Regarding nanoparticle-polymer interactions, the favorable enthalpy change ($\Delta H < 0$) triumphed over the unfavorable entropy

loss ($\Delta S < 0$) [24], which is consistent with the findings of previous research [25, 26]. The change of enthalpy and entropy corresponds to a general predominance of electrostatic interactions and van der Waals interactions[27]. The change of Gibbs energy (-26.3 ± 0.1 kJ/mol for AD and -22.6 ± 0.5 kJ/mol for ADS) reflected that the interaction between polymers (AD and ADS) and insulin nanoparticles were energetically favorable at 25 °C (**Figure 1**h). The calculated number of ADS molecules adsorbed onto insulin nanoparticles (17.1 ± 2.5 per 10 nm^2) was significantly ($P < 0.01$) larger than that of AD (6.1 ± 0.7 per 10 nm^2, **Figure 1**i).

With the help of ADS, the size of insulin particles decreased from 1217.7 ± 234.3 to 382.0 ± 10.6 nm (**Figure 1**j); meanwhile the polydispersity index was improved from 0.22 ± 0.08 to 0.08 ± 0.01 (**Figure 1**k). Zeta potential of insulin nanoparticles increased from 13.1 ± 2.2 to 25.1 ± 2.8 mV after ADS adsorption (**Figure 1**l). No such size decrease, dispersity improvement and zeta potential increase were observed for the addition of AD. Benefiting from surface camouflage with ADS, insulin nanoparticles can be well-dispersed in the oil phase together with ADS.

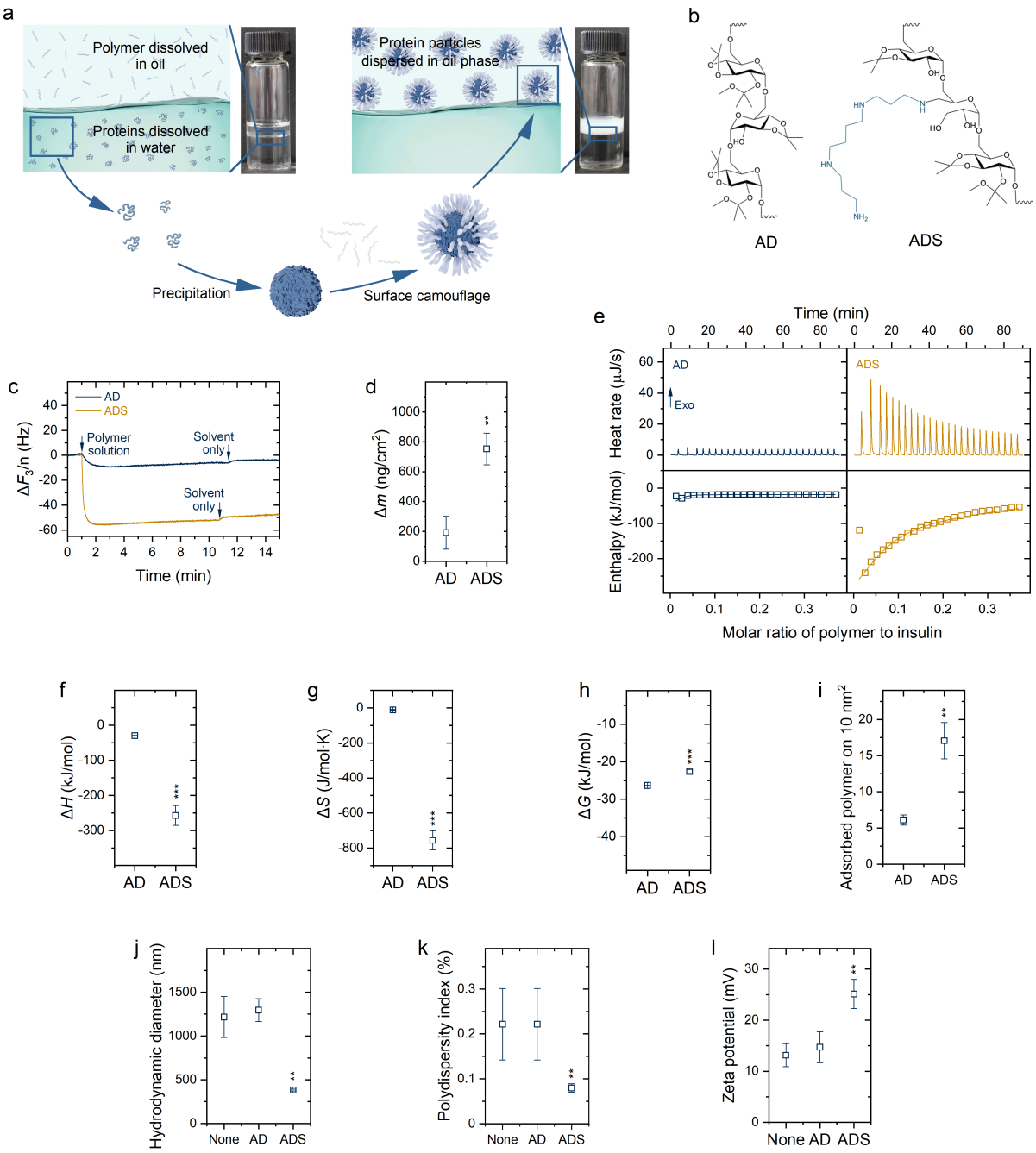

Figure 1. **Surface camouflage of insulin nanoparticles.** (**a**) Scheme of surface camouflage. After surface camouflage with carrier materials, protein nanoparticles tend to stay within the oil phase. (**b**) Molecule structure of AD and ADS. (**c**) Normalized frequency (Δf/n) of the third overtone as a function of time when polymer solution flew over a quartz disc coated with insulin nanoparticles. (**d**) The adsorbed mass (Δ*m*) of AD and ADS on the insulin nanoparticle-coated quartz disc (*n*=3). (**e**) Isothermal titration calorimetry titration of AD or ADS into insulin nanoparticle suspension. The top panels show the raw data before the subtraction of

background enthalpograms for polymer dilution. The bottom panels show the isotherms created by plotting the integrated heat peaks against the molar ratio of the polymer. (**f-h**) The enthalpy (f), entropy (g) and Gibbs energy (h) change of the interaction between polymers (AD and ADS) and insulin nanoparticles deduced from the isothermal titration calorimetry enthalpograms (n=3). (**i**) The adsorbed number of AD or ADS molecules onto per 10 nm^2 surface area of insulin nanoparticles deduced from the isothermal titration calorimetry enthalpograms (n=3). (**j** and **k**) The hydrodynamic diameter (j) and polydispersity index (k) of insulin particles before and after adding AD or ADS (n=3). (**l**) The zeta potential of insulin particles before and after adding AD or ADS (n=3). The term None refers to the group without polymers. The AD and ADS group were compared with the None group. The levels of significance were set at probabilities of $^{**}P < 0.01$, and $^{***}P < 0.001$.

Secondly, we performed molecular dynamics simulations to probe the mechanisms of carrier material-insulin interaction. It is a challenge to simulate and to verify the surface structure of nanoparticle in amorphous state. Therefore, instead of an insulin nanoparticle, one insulin molecule was selected to perform the simulation. To distinguish the effect of potential functional groups, we selected ADS-1 (one glucose unit with one spermine group) and ADS-3 (three glucose units with one spermine group) as the carrier materials (**Figure S2**). The corresponding AD molecules (AD-1 and AD-3) served as controls.

Simulation of the one-to-one interaction between a polymer molecule and an insulin molecule was conducted to predict their preferred orientation in the complex (**Figure S3**). AD-1 and AD-3 escaped from their corresponding initial complexes, meanwhile, ADS-1 and ADS-3 were always in contact with the insulin molecule (**Figure 2**a). As expected, the root-mean-square deviation (RMSD) value (**Figure 2**b) fluctuated widely for the complex containing AD-1 (from 1.6 Å to 41.9 Å) and AD-3 (from 1.7 Å to 40.4 Å). In contrast, the maximum RMSD

value < 8 Å for the complex with ADS-1 and ADS-3, and these complexes remained compact up to 150 ns. According to the RMSD plot, the complexes containing ADS-1 and ADS-3 were reasonably more stable than those with AD molecules. The contribution of electrostatic force and Van der Waals force for complexes containing ADS was significantly higher than those containing AD (**Figures 2**c and **2**d). Regardless of polymer types, the contribution of electrostatic force was always larger than that offered by van der Waals force.

Multi-to-one simulations were conducted to distinguish the residues in an insulin molecule that contributed to the interaction with polymers (**Figure S4**). With three ADS-3 molecules, only two of them complexed with the insulin molecule (**Figure S**5). When only two polymer molecules added, both ADS-3 molecules were compacted with the insulin molecule after 700 ns simulation, meanwhile, AD-3 molecules were scattered around the insulin molecule (**Figure 2**e). The radial distribution density of ADS-3 around the insulin molecule climbed to 547 μg/cm^3 as the distance increased to 5 Å, while AD-3 barely distributed within 5 Å from the insulin molecule (**Figure 2**f). This process can also be tracked by examining the numbers of contact points (within 4 Å) between polymer and insulin molecules [28]. No contact points were detected between AD-3 and insulin over the whole simulation process (**Figure 2**g). For the complex containing ADS-3, the number of contact points increased sharply after 168 ns simulation and the maximum number was 196. Regarding the insulin molecule, GLY_41 and GLU_42 possessed the largest number of contacts with ADS-3, fluctuating within a range between 1 and 50 (**Figure 2**h). To be noted that, apart from the interaction between polymer monomers and insulin residues, the entropic repulsion among polymer monomers may also affect the surface adsorption of polymer molecules [29]. Since the surface bends toward polymer molecules, curved surface for insulin nanoparticles may facilitate the polymer adsorption [29, 30].

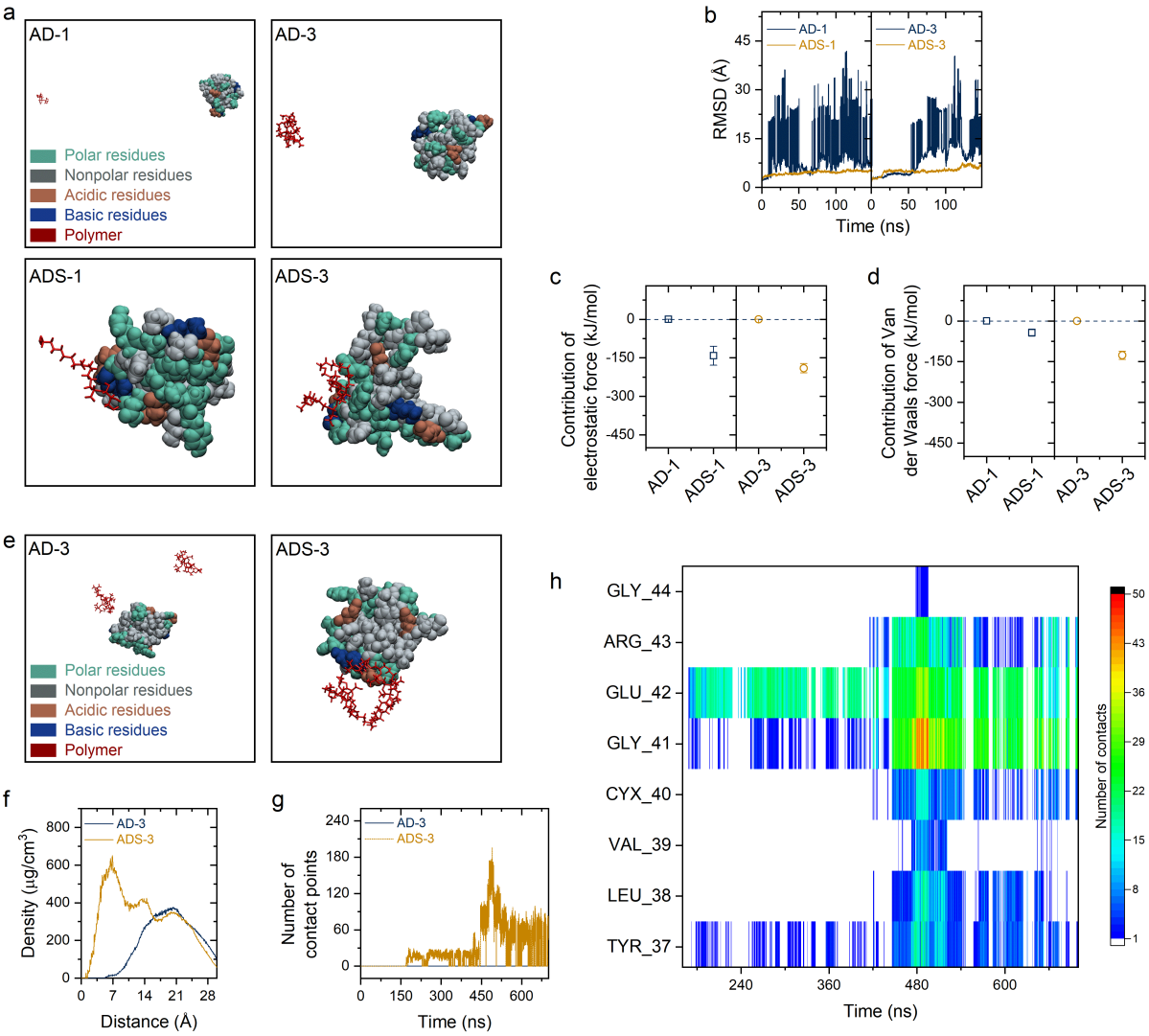

Figure 2. Molecular dynamics simulations of the interactions between polymer and insulin molecules. (**a**) Snapshots of one polymer molecule complexed with one insulin molecule (1:1) after 150 ns simulation. Solvent molecules were hidden for clarity. (**b**) RMSD for the complexation between polymer and insulin molecules (1:1) over 150 ns simulation. (**c** and **d**) The corresponding contributions of electrostatic force (c) and van der Waals force (d) of the polymer and insulin molecule complexation (1:1). (**e**) Snapshots of two polymer molecules complexed with one insulin molecule (2:1) after 700 ns simulation. Solvent molecules were hidden for clarity. (**f**) The density variation of AD-3 and ADS-3 as a function of the distance from the insulin molecule. (**g**) Variation of the number of contact points between two polymer molecules and one insulin molecule within 4 Å. (**h**) Heat map of interaction of

ADS with residues of insulin over 700 ns simulation. The color bar on the right side represents the number of contact points (1−50).

Thirdly, we argue that the solidification of adsorbed polymer molecules can cover the surface of insulin nanoparticles. This surface coverage is feasible to inhibit the phase transfer of insulin nanoparticles and achieve ultrahigh efficient encapsulation of insulin, as long as the solidified polymer layer remains compacted. To verify this hypothesis, we "pulled" insulin nanoparticles from oil phase to water phase by centrifugation using a swing-bucket rotor (**Figure 3**a). To facilitate the phase transfer of nanoparticles by centrifugation, ethyl acetate (0.902 g/cm^3 at 25 °C), a water-immiscible solvent with a density lighter than that of water (0.997 g/cm^3 at 25 °C), was selected to suspend insulin nanoparticles. When only insulin nanoparticles (10 mg/mL) were dispersed in oil phase, the milky appearance of oil phase disappeared after centrifugation (8×*g*), indicating the transfer of insulin nanoparticles to water phase (**Figure 3**b). No pellets were observed at the bottom of containers after centrifugation, which can be ascribed to the high water-solubility of insulin. It is worth noting that the apparent water solubility of insulin was improved (> 15 mg/mL in 1 h at 25 °C) after forming nanoparticles in acetone. The AD group showed a similar phenomenon with the group without any polymers, suggesting that AD molecules (10 mg/mL) had no effects on the phase transfer of insulin nanoparticles. Unlike the AD group, there is no obvious change in the milky appearance of oil phase after centrifugation for the ADS group (10 mg/mL).

We evaluated the impact of insulin-polymer weight ratios on the phase transfer of insulin nanoparticles under centrifugation (8×*g*; **Figure 3**c). Regardless of weight ratios, the fraction of insulin nanoparticles dissolved in water phase fluctuated between 72% and 87% for groups without polymers and with AD molecules. Insulin molecules was barely detected in water phase for the ADS group. For example, with an insulin-ADS weight ratio of 5:5, ADS successfully reduced the insulin dissolved in water phase to be smaller than 1%. It seemed that

the surface camouflage with ADS was capable to keep insulin nanoparticles in oil phase after centrifugation (8×*g*).

When the centrifugal force was higher than 805×*g*, white pellets were formed at the bottom of the containers (**Figure 3**d). Regardless of the centrifugal force, only less than 0.01% of insulin was detected in water phase at an insulin-ADS weight ratio of 4:6 (**Figure 3**e). By increasing the weight ratio to 7:3, only 0.3%-2.8% of insulin was dissolved in water phase. For insulin-ADS weight ratios of 4:6, 5:5, 6:4 and 7:3, the increase of centrifugal force just slightly increased the fraction of insulin dissolved in water phase. At the 8:2 weight ratio, the fraction of insulin dissolved in water phase was continually increased from 1.4% to 8.2% when the centrifugal force was increased from 50×*g* to 3220×*g*. With the insulin-ADS weight ratio up to 8:2 and centrifugal force up to 3220×*g*, the fraction of insulin dissolved in water was less than 10%, revealing the power of ADS in inhibiting the insulin phase transfer into water phase. It seemed that the surface camouflage with ADS was capable to isolate insulin nanoparticles from water phase. A possible explanation might be that the adsorbed ADS fully covered the surface of insulin nanoparticles. By transferring the ADS-camouflaged insulin nanoparticles into water phase, ADS formed a compact layer onto the surface of insulin nanoparticles, which is sufficient to inhibit the insulin phase transfer and avoid the leakage of insulin to water phase.

Insulin-encapsulated microcomposites, insulin@ADS, were engineered using a flow-focusing device (**Figure 3**f and **Figure S6**). The dispersed (oil) phase, an ADS dimethyl carbonate solution containing insulin nanoparticles, was emulsified by a continuous phase (polyvinyl alcohol solution; 1 %, w/v). Regardless of the studied insulin-ADS weight ratios, all the obtained microcomposites were spherical (**Figures 3**g and **S7**). As the insulin-ADS weight ratio increased from 4:6 to 8:2, the corresponding encapsulation efficiency (percentage of insulin loaded relative to the total amount of insulin) fluctuated within a range between 98.3% and 99.9% (**Figure 3**h). This value decreased to 64.4% when the insulin-ADS weight ratio

increased to 9:1. The insulin loading degree (mass fraction of insulin in microcomposites) was up to 76.6%. Such loading degree values are ultrahigh for protein-encapsulated microcomposites, which can be ascribed to the surface camouflage of insulin nanoparticles. In comparison with the molecular level modification, nanoparticle surface camouflage approach greatly reduced the amount of carrier materials and, therefore, achieved ultrahigh mass fraction of insulin in microcomposites.

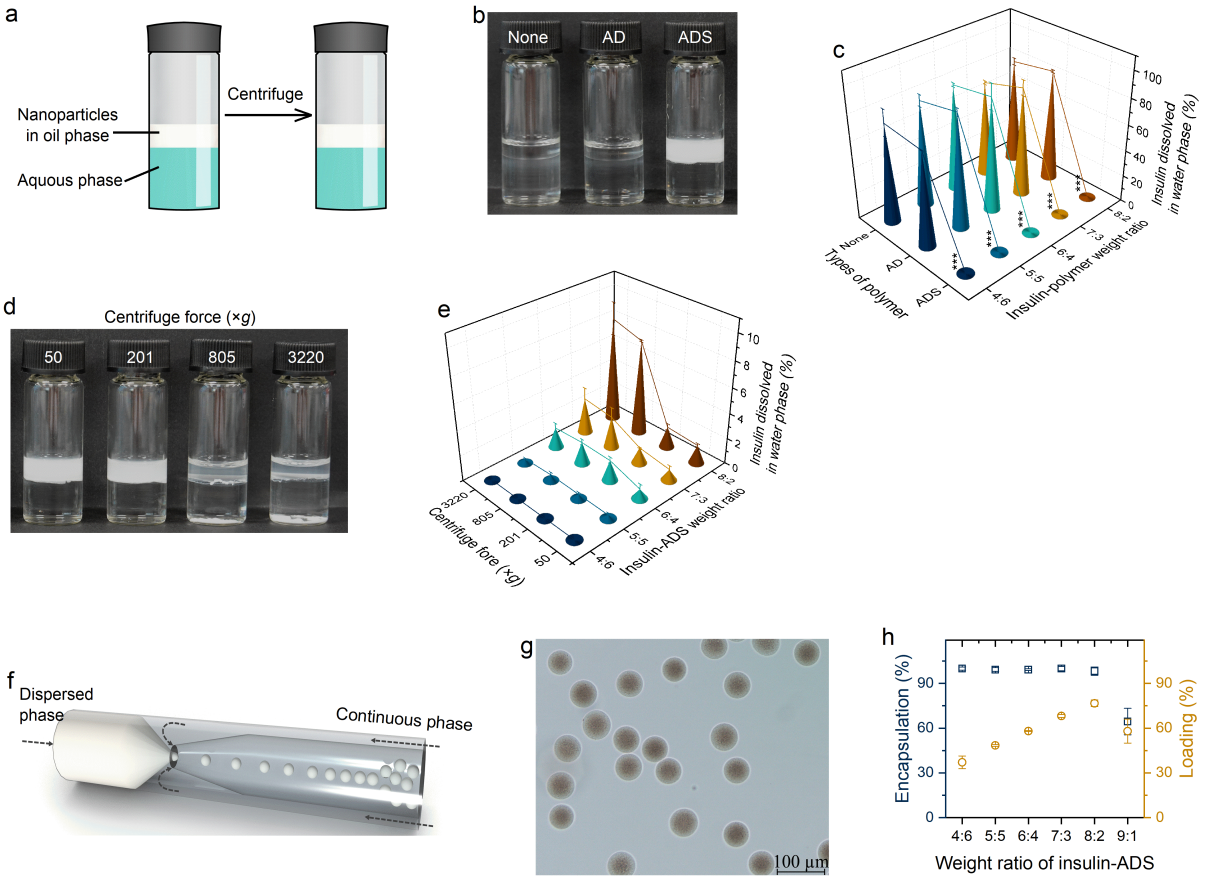

Figure 3. **Efficient insulin encapsulation through surface camouflage.** (**a**) Evaluation of surface camouflage on the phase transfer of insulin nanoparticles using a swing-bucket rotor. (**b**) A representative photograph of two-phase systems after phase transfer by centrifugation at 8×*g* for 5 min. Oil phase containing insulin nanoparticles (10 mg/mL) and polymers (AD or ADS, 10 mg/mL) stacked on the surface of water phase. (**c**) The effect of polymers (AD and ADS) and insulin-polymer weight ratio on the percentage of insulin nanoparticles dissolved in

water phase after centrifugation at 8×*g* for 5 min (*n*=3). The overall concentration of insulin and polymers was set at 20 mg/mL. (**d**) A representative photograph of two-phase systems after centrifugation under different centrifugal forces. Oil phase containing insulin nanoparticles (10 mg/mL) and ADS (10 mg/mL) stacked on the surface of water phase. (**e**) The effect of insulin-ADS weight ratio and centrifugal force on the percentage of insulin nanoparticles dissolved in water phase after centrifugation (*n*=3). (**f**) The schematic of flow-focusing device for insulin@ADS microcomposite preparation. (**g**) The light microscope image of insulin@ADS with a 5:5 insulin-ADS weight ratio. (**h**) The effect of insulin-ADS weight ratio on the insulin encapsulation efficiency and insulin loading degree in ADS microcomposites (*n*=3). The term None refers to the group without polymers. The AD and ADS groups were compared with the None group; the levels of significance were set at probabilities of $^{***}P < 0.001$.

Fourthly, to verify the versatility of our surface camouflage strategy, we studied the surface adsorption of polymer molecules on albumin (bovine serum albumin), β-LG and ovalbumin nanoparticles, which have abundant acid residues and might have strong electrostatic attraction with ADS. As shown in **Figure 4**a, the adsorbed mass of ADS and solvent molecules on the surface of albumin (666.1 ± 103.7 ng/cm^2), β-LG (726.8 ± 66.3 ng/cm^2) and ovalbumin (608.2 ± 81.9 ng/cm^2) layers was significantly higher than that of AD (306.5 ± 42.1, 168.2 ± 50.9 and 230.1 ± 29.4 ng/cm^2 for albumin, β-LG and ovalbumin, respectively). After surface camouflage, ADS stabilized albumin, β-LG and ovalbumin particles, whose size decreased to 267.9 ± 23.9, 169.1 ± 4.4 and 161.3 ± 13.0 nm, respectively (**Figure 4**b). The polydispersity index for albumin, β-LG and ovalbumin nanoparticles in dimethyl carbonate improved to be 0.06 ± 0.03, 0.04 ± 0.01 and 0.20 ± 0.03, respectively (**Figure 4**c). With the camouflage of ADS, the zeta potential of albumin, β-LG and ovalbumin nanoparticles increased obviously from -29.5 ± 0.9, -40.5 ± 0.9 and -31.0 ± 4.1 mV to -6.1 ± 0.1, -15.1 ± 1.5 and -14.9 ± 2.1 mV, respectively (**Figure 4**d).

We also "pulled" albumin, β-LG and ovalbumin nanoparticles (10 mg/mL) from oil phase to water phase by centrifugation. With the help of ADS (10 mg/mL), less than 2 % of albumin, β-LG and ovalbumin crossed the interface and dissolved in the water phase after centrifugation at 8×*g* for 5 min (**Figures 4**e and f). Without any polymers, > 90% of albumin and β-LG nanoparticles dissolved in the water phase. With the addition of AD, 90.5 ± 3.7% of albumin was detected in water phase after centrifugation at 8×*g*, while only 3.8 ± 2.6% of β-LG was measured in the water phase. However, after increasing the centrifugal force to 3229×*g*, almost all the β-LG nanoparticles (95.5 ± 2.6%; data not shown) dissolved in the water phase. For groups without polymers or with AD, only 20.7 ± 0.8% and 20.5 ± 1.5%, respectively, of ovalbumin nanoparticles dissolved in the water phase after centrifugation at 8×*g*, which presumably due to the reduced water solubility of ovalbumin nanoparticles. With the help of ADS surface camouflage, albumin, β-LG or ovalbumin molecules (< 0.6%) were barely detected in water phase (**Figures 4**g and **4**h), even we increased the centrifugal force to 3220×*g*. We engineered albumin-, β-LG- or ovalbumin-encapsulated microcomposites with a protein-ADS weight ratio of 5:5. As expected, the ultrahigh protein encapsulation (> 97%) was observed for all microcomposites with the protein loading degrees close to 50% (**Figure 4**i). Collectively, the results of albumin, β-LG and ovalbumin verified the feasibility and versatility of our camouflage strategy for protein encapsulation.

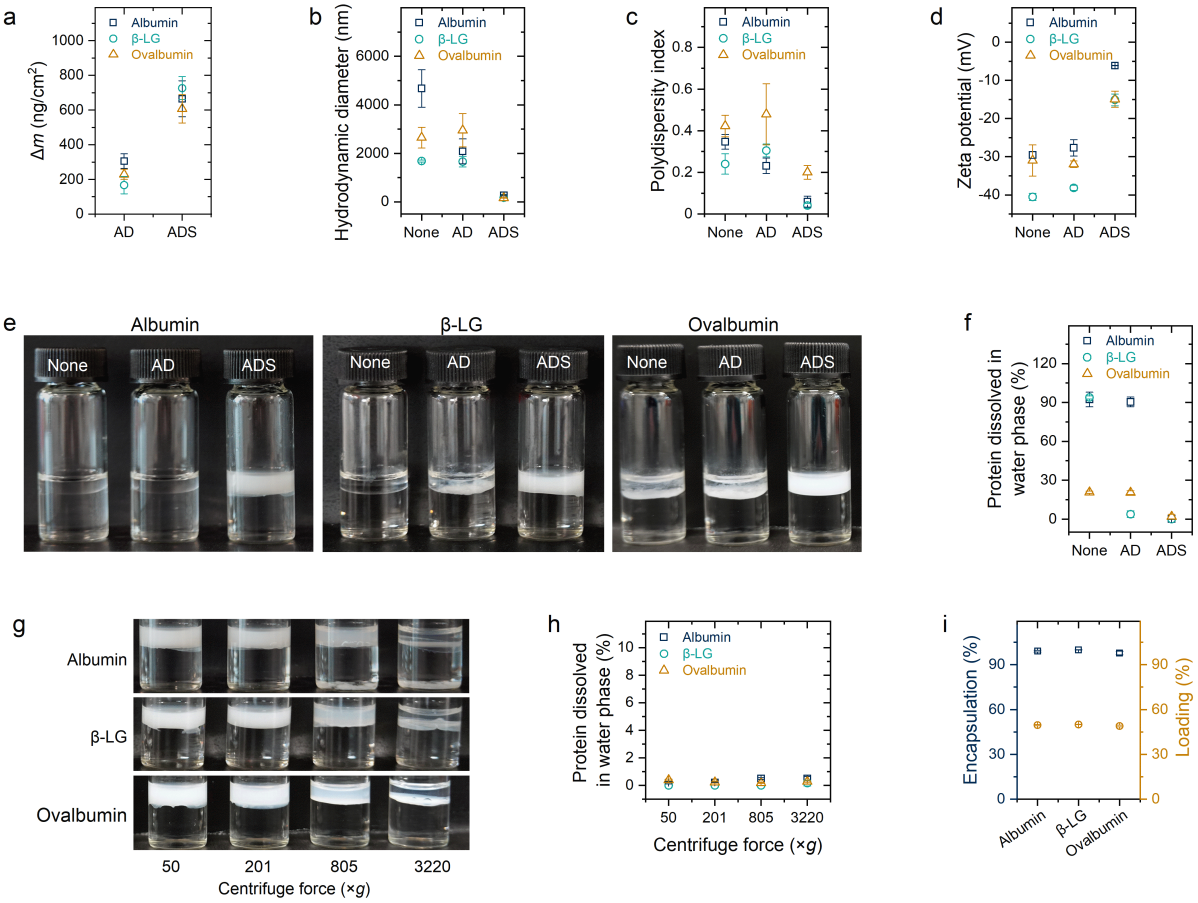

Figure 4. Versatility of camouflage strategy for efficient encapsulation. (**a**) The calculated adsorbed mass (Δ*m*) of polymers on albumin, β-LG or ovalbumin nanoparticle-coated quartz disc (*n*=3). (**b** and **c**) The hydrodynamic diameter (b) and polydispersity index (c) of albumin, β-LG and ovalbumin particles with and without polymers (*n*=3). (**d**) The zeta potential of albumin, β-LG and ovalbumin particles with and without polymers (*n*=3). (**e**) Representative photographs of two-phase systems after phase transfer by centrifugation at 8×*g* for 5 min. Oil phase containing albumin, β-LG or ovalbumin nanoparticles (10 mg/mL) and polymers (AD or ADS, 10 mg/mL) stacked on the surface of water phase. (**f**) The effect of polymers (10 mg/mL) on the percentage of albumin, β-LG and ovalbumin nanoparticles (10 mg/mL) dissolved in water phase after centrifugation at 8×*g* for 5 min (*n*=3). (**g**) Representative photographs of two-phase systems after centrifugation under different centrifugal forces. Oil phase containing albumin, β-LG or ovalbumin nanoparticles (10 mg/mL) and ADS (10 mg/mL) stacked on the surface of water phase. (**h**) Quantitative analysis of albumin, β-LG and

ovalbumin nanoparticles dissolved in water phase under different centrifugal forces (*n*=3). The concentrations for albumin nanoparticles, β-LG nanoparticles, ovalbumin nanoparticles and ADS were all fixed at 10 mg/mL. (**i**) Drug encapsulation efficiency and drug loading degree of albumin, β-LG and ovalbumin in ADS microcomposites with a weight ratio of 5:5 between proteins (albumin, β-LG or ovalbumin) and ADS (*n*=3). The term None refers to the group without polymers.

At last, we verified the glycemic control capability of insulin@ADS (insulin-ADS weight ratio of 5:5) on streptozotocin-induced type 1 diabetic Sprague–Dawley rats (**Figure 5**a) [31-37]. For insulin nanoparticles, approximately 99.0% of insulin released within 0.25 day (**Figure 5**b). In contrast, the fraction of insulin released from insulin@ADS was approximately 5.2% over the first day. The engineered microcomposites enabled the sustained release of insulin for up to 25 days (**Figure 5**c). By increasing the insulin-ADS ratio from 4:6 to 8:2, the released fraction of insulin climbed from approximately 5.1% to approximately 40.8% at the first day of the release study (**Figure S**8). High drug loading degree could adversely affect the release profiles of microcomposites [38]. All types of microcomposites successfully enabled the gradual release of insulin molecules, which can be ascribed to the layer of ADS molecules on each protein nanoparticle. After solidification, this ADS layer efficiently prolonged the payload release.

The circular dichroism spectrum of the released insulin agreed with that of native insulin (**Figure 5**d). The ratio of molar ellipticity between the bands at 208 nm and 223 nm, [Φ]208/[Φ]223, is a qualitative indicator toward the overall conformation of insulin molecules [39, 40]. The [Φ]208/[Φ]223 for the released insulin (1.39) was quite close to that of native insulin (1.29), indicating negligible conformational change during the encapsulation and release process. Moreover, the encapsulated insulin was maintained in amorphous state (**Figure S9**).

Insulin@ADS increased serum insulin level for more than 14 days with a peak (approximately 95 mUI/L) at 12 hours after administration (**Figure 5**e). For insulin solution group, the serum insulin level reached a peak (approximately 132 mUI/L) within 2 h after administration and declined rapidly (**Figure 5**f). Although the dose of insulin@ADS was 5 times of insulin solution, the maximum plasma concentration for insulin@ADS was significantly lower than that of insulin solution. The smaller maximum plasma concentration for insulin@ADS demonstrated its capability of controlling the release of payloads with high mass fraction of therapeutics. After encapsulation in ADS microcomposites, the half-life of insulin was significantly ($P < 0.001$) prolonged from approximately 0.2 to 4.0 days (**Figure 5**g); the mean residence time was 42.4 times ($P < 0.001$) higher than that of insulin solution (**Figure 5**h). The area under the curve for insulin solution and insulin@ADS group was 14.1 ± 4.2 and 381.3 ± 71.0 mIU/L·day, respectively (**Figure 5**i). Considering the dose given, the bioavailability of insulin@ADS was 4.4 times higher than that of the corresponding insulin solution.

Insulin@ADS reduced the blood glucose level to normal range within 1 day, and attained tight glycemic control for up to 14 days (**Figure 5**j). This glycemic control duration decreased to 10 days when the insulin-ADS weight ratio increased to 6:4 or 7:3 (**Figure S10**). The blood glucose level of rats treated with insulin solution returned to their initially hyperglycemic state within 6 h. The glycemic control ability of insulin solution and insulin@ADS was in accordance with their pharmacokinetic results. Normal saline and bare ADS microparticles did not show any influence on the blood glucose levels (**Figure S11**). Moreover, insulin@ADS inhibited body weight loss, one of the clinical symptoms for type I diabetes (**Figure S12**). Both the density of CD68 (macrophage marker) positive cells around the injection site, and the hematoxylin and eosin staining results verified the good biocompatibility of the insulin@ADS (**Figures S13** and **S14**). Overall, insulin@ADS with insulin-ADS weight ratio of 5:5

successfully increased the serum insulin level and efficiently reduced the blood glucose for 14 days. Consequentially, insulin@ADS was capable to decrease the injection frequency of insulin, and to improve the compliance of patients and treatment efficacy.

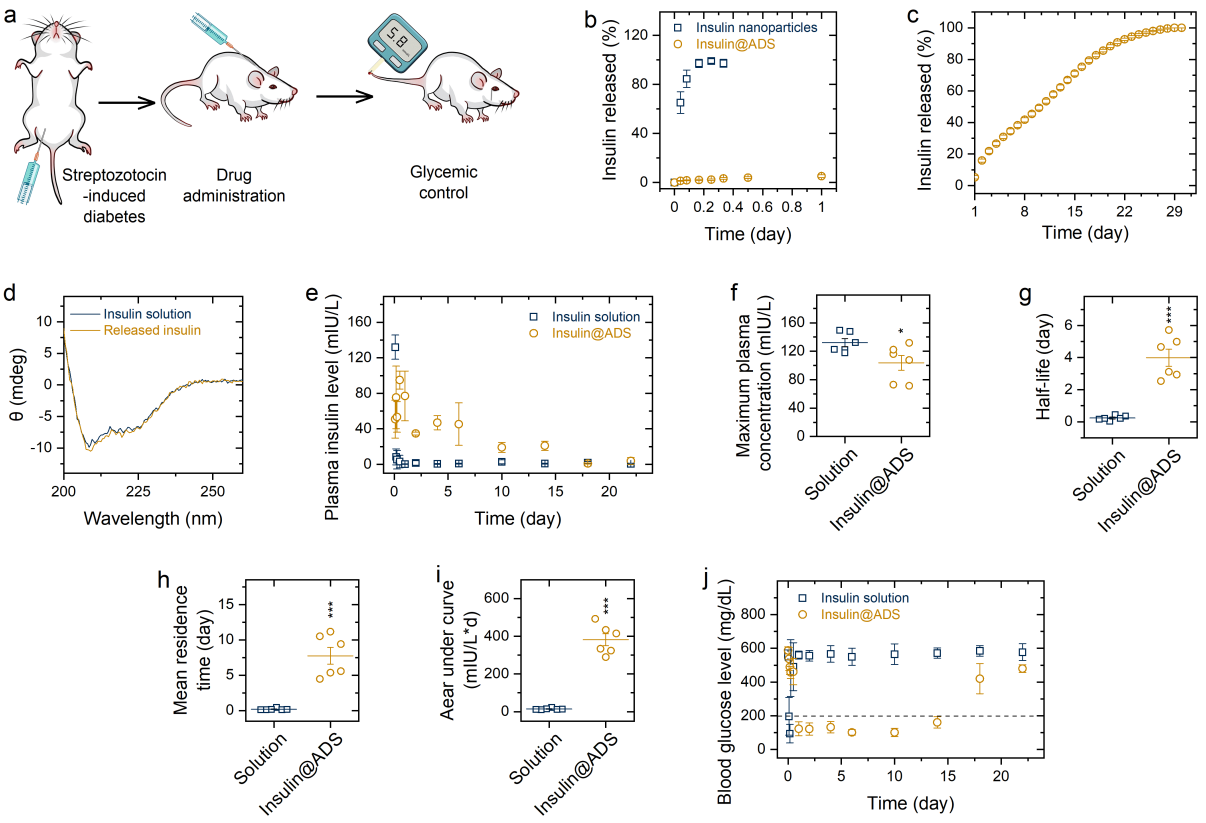

Figure 5. Microcomposites persist two weeks in rats for diabetes therapy. (**a**) Schematic illustration of *in vivo* experiment. (**b** and **c**) The first day release profiles of insulin nanoparticles and insulin@ADS with insulin-ADS weight ratio of 5:5 (b) and the release profiles after the first day (c; *n*=3). (**d**) Circular dichroism spectra of native insulin and released insulin. (**e**) Plasma insulin concentration of rats treated with insulin solution and insulin@ADS with insulin-ADS weight ratio of 5:5 (*n*=6). (**f-i**) The maximum plasma concentration (f), half-life (g), mean residence time (h) and area under curve (i) of insulin solution and insulin@ADS with insulin-ADS weight ratio of 5:5 calculated from the curve of plasma insulin level versus time (*n*=6). (**j**) Blood glucose levels of rats treated with insulin solution and insulin@ADS with

insulin-ADS weight ratio of 5:5 (n=6). Insulin@ADS was compared with the solution; the level of significance was set at probabilities of $^{*}P < 0.05$, and $^{***}P < 0.001$.

In summary, we successfully develop a versatile surface camouflage strategy to efficiently encapsulate water-soluble proteins. By formulating proteins into nanoparticles, this strategy transforms the demand of molecular modification to the more prevalent surface camouflage of protein nanoparticles. The main driving forces for the protein nanoparticle-polymer interactions are electrostatic attraction and van der Waals forces. This camouflage enables the dispersion of protein nanoparticles in oil phase, addressing the miscibility issue between the protein and carrier materials. The adsorbed ADS layer is compact enough to inhibit phase transfer and minimize the leakage of insulin, albumin, β-lactoglobulin and ovalbumin into water phase. In comparison with the molecular level camouflage, nanoparticle surface camouflage greatly reduces the amount of carrier materials and, therefore, achieving ultrahigh drug loading degrees up to 77%. The prepared insulin@ADS maintains blood glucose level of hyperglycemic rats within the normal range for 14 days after a single injection. Overall, the surface camouflage is a versatile strategy that can engineer systems simultaneously featured with ultrahigh mass fraction of proteins and controlled drug release profiles.

Acknowledgements

We acknowledge the financial support from Natural Science Foundation of China (No. 51903251, 81973266, 81772352 and 82072437), Academy of Finland (No. 322093 and 308742), Natural Science Foundation of Jiangsu Province (No. BK20190554), National Mega-project for Innovative Drugs (2019ZX09721001), Education Department of Liaoning Provence (2020LJC04), University of Helsinki Research Funds, HiLIFE Research Funds, and Natural Science Foundation for Distinguished Young Scholars of Jiangsu Province (BK20190032).

Supporting Information

Experimental methods, supplementary figures and additional discussions. This material is available free of charge at http://pubs.acs.org.

Reference

1. Augustin, M. A.; Hemar, Y., Nano-and Micro-Structured Assemblies for Encapsulation of Food Ingredients. *Chemical Society Reviews* **2009,** *38* (4), 902-912.

2. Fernandes, R.; Gracias, D. H., Self-Folding Polymeric Containers for Encapsulation and Delivery of Drugs. *Advanced Drug Delivery Reviews* **2012,** *64* (14), 1579-1589.

3. Wei, T. H.; Wu, S. H.; Huang, Y. D.; Lo, W. S.; Williams, B. P.; Chen, S. Y.; Yang, H. C.; Hsu, Y S.; Lin, Z. Y.; Chen, X. H., Rapid Mechanochemical Encapsulation of Biocatalysts into Robust Metal–Organic Frameworks. *Nature Communications* **2019,** *10* (1), 1-8.

4. Anderson, J. M.; Shive, M. S., Biodegradation and Biocompatibility of Pla and Plga Microspheres. *Advanced Drug Delivery Reviews* **2012,** *64*, 72-82.

5. Hamdy, S.; Haddadi, A.; Hung, R. W.; Lavasanifar, A., Targeting Dendritic Cells with Nano-Particulate Plga Cancer Vaccine Formulations. *Advanced Drug Delivery Reviews* **2011,** *63* (10-11), 943-955.

6. Li, J.;Wang, X.; Zhang, T.; Wang, C.; Huang, Z.; Luo, X.; Deng, Y., A Review on Phospholipids and Their Main Applications in Drug Delivery Systems. *Asian Journal of Pharmaceutical Sciences* **2015,** *10* (2), 81-98.

7. McClements, D. J., Recent Developments in Encapsulation and Release of Functional Food Ingredients: Delivery by Design. *Current Opinion in Food Science* **2018,** *23*, 80-84.

8. Hofmeister, I.; Landfester, K.; Taden, A., Ph-Sensitive Nanocapsules with Barrier Properties: Fragrance Encapsulation and Controlled Release. *Macromolecules* **2014,** *47* (16), 5768-5773.

9. Zhuang, J.; Kuo, C. H.; Chou, L. Y.; Liu, D. Y.; Weerapana, E.; Tsung, C. K., Optimized Metal–Organic-Framework Nanospheres for Drug Delivery: Evaluation of Small-Molecule Encapsulation. *ACS Nano* **2014,** *8* (3), 2812-2819.

10. Jiang, Y.; Qiu, L.; Juarez-Perez, E. J.; Ono, L. K.; Hu, Z.; Liu, Z.; Wu, Z.; Meng, L.; Wang, Q.; Qi, Y., Reduction of Lead Leakage from Damaged Lead Halide Perovskite Solar Modules Using Self-Healing Polymer-Based Encapsulation. *Nature Energy* **2019,** *4* (7), 585-593.

11. Putney, S. D.; Burke, P. A., Improving Protein Therapeutics with Sustained-Release Formulations. *Nature Biotechnology* **1998,** *16* (2), 153-157.

12. Liu, J.; Xiao, Y.; Allen, C., Polymer–Drug Compatibility: A Guide to the Development of Delivery Systems for the Anticancer Agent, Ellipticine. *Journal of Pharmaceutical Sciences* **2004,** *93* (1), 132-143.

13. Zhang, Y.; Ren, T.; Gou, J.; Zhang, L.; Tao, X.; Tian, B.; Tian, P.; Yu, D.; Song, J.; Liu, X., Strategies for Improving the Payload of Small Molecular Drugs in Polymeric Micelles. *Journal of Controlled Release* **2017,** *261*, 352-366.

14. Letchford, K.; Liggins, R.; Burt, H., Solubilization of Hydrophobic Drugs by Methoxy Poly (Ethylene Glycol)-Block-Polycaprolactone Diblock Copolymer Micelles: Theoretical and Experimental Data and Correlations. *Journal of Pharmaceutical Sciences* **2008,** *97* (3), 1179-1190.

15. Manoharan, C.; Singh, J., Insulin Loaded Plga Microspheres: Effect of Zinc Salts on Encapsulation, Release, and Stability. *Journal of Pharmaceutical Sciences* **2009,** *98* (2), 529-542.

16. Lv, S.; Wu, Y.; Cai, K.; He, H.; Li, Y.; Lan, M.; Chen, X.; Cheng, J.; Yin, L., High Drug Loading and Sub-Quantitative Loading Efficiency of Polymeric Micelles Driven by Donor–Receptor Coordination Interactions. *Journal of the American Chemical Society* **2018,** *140* (4), 1235-1238.

17. Leunissen, M.E.; Van Blaaderen, A.; Hollingsworth, A. D.; Sullivan, M. T.; Chaikin, P. M., Electrostatics at the Oil–Water Interface, Stability, and Order in Emulsions and Colloids. *Proceedings of the National Academy of Sciences* **2007,** *104* (8), 2585-2590.

18. Yethiraj, A.; van Blaaderen, A., A Colloidal Model System with an Interaction Tunable from Hard Sphere to Soft and Dipolar. *Nature* **2003,** *421* (6922), 513-517.

19. Leunissen, M. E.; Christova, C. G.; Hynninen, A. P.; Royall, C. P.; Campbell, A. I.; Imhof, A.; Dijkstra, M.; Van Roij, R.; Van Blaaderen, A., Ionic Colloidal Crystals of Oppositely Charged Particles. *Nature* **2005,** *437* (7056), 235-240.

20. Cohen, J. L.; Schubert, S.; Wich, P. R.; Cui, L.; Cohen, J. A.; Mynar, J. L.; Fréchet, J. M., Acid-Degradable Cationic Dextran Particles for the Delivery of Sirna Therapeutics. *Bioconjugate Chemistry* **2011,** *22* (6), 1056-1065.

21. Matteucci, E.; Giampietro, O.; Covolan, V.; Giustarini, D.; Fanti, P.; Rossi, R., Insulin Administration: Present Strategies and Future Directions for a Noninvasive (Possibly More Physiological) Delivery. *Drug Design, Development and Therapy* **2015,** *9*, 3109.

22. Hung, Y. T.; Lin, M. S.; Chen, W. Y.; Wang, S. S., Investigating the Effects of Sodium Dodecyl Sulfate on the Aggregative Behavior of Hen Egg-White Lysozyme at Acidic Ph. *Colloids Surf B Biointerfaces* **2010,** *81* (1), 141-151.

23. Roselin, L. S.; Lin, M. S.; Lin, P. H.; Chang, Y.; Chen, W. Y., Recent Trends and Some Applications of Isothermal Titration Calorimetry in Biotechnology. *Biotechnology Journal: Healthcare Nutrition Technology* **2010,** *5* (1), 85-98.

24. Huang, R.; Lau, B. L. T., Biomolecule–Nanoparticle Interactions: Elucidation of the Thermodynamics by Isothermal Titration Calorimetry. *Biochimica et Biophysica Acta (BBA) - General Subjects* **2016,** *1860* (5), 945-956.

25. Winzen, S.; Schoettler, S.; Baier, G.; Rosenauer, C.; Mailaender, V.; Landfester, K.; Mohr, K., Complementary Analysis of the Hard and Soft Protein Corona: Sample Preparation Critically Effects Corona Composition. *Nanoscale* **2015,** *7* (7), 2992-3001.

26. Müller, J.; Simon, J.; Rohne, P.; Koch-Brandt, C.; Mailänder, V.; Morsbach, S.; Landfester, K., Denaturation Via Surfactants Changes Composition of Protein Corona. *Biomacromolecules* **2018,** *19* (7), 2657-2664.

27. Prozeller, D.; Morsbach, S.; Landfester, K., Isothermal Titration Calorimetry as a Complementary Method for Investigating Nanoparticle–Protein Interactions. *Nanoscale* **2019,** *11* (41), 19265-19273.

28. Best, R. B.; Hummer, G.; Eaton, W. A., Native Contacts Determine Protein Folding Mechanisms in Atomistic Simulations. *Proceedings of the National Academy of Sciences* **2013,** *110* (44), 17874-17879.

29. Hershkovits, E.; Tannenbaum, A.; Tannenbaum, R., Polymer Adsorption on Curved Surfaces: A Geometric Approach. *The Journal of Physical Chemistry C* **2007,** *111* (33), 12369-12375.

30. Wagner, J.; Erdemci-Tandogan, G.; Zandi, R., Adsorption of Annealed Branched Polymers on Curved Surfaces. *Journal of Physics: Condensed Matter* **2015,** *27* (49), 495101.

31. Park, W.; Kim, D.; Kang, H. C.; Bae, Y. H.; Na, K., Multi-Arm Histidine Copolymer for Controlled Release of Insulin from Poly (Lactide-Co-Glycolide) Microsphere. *Biomaterials* **2012,** *33* (34), 8848-8857.

32. Tauschmann, M.; Thabit, H.; Bally, L.; Allen, J. M.; Hartnell, S.; Wilinska, M. E.; Ruan, Y.; Sibayan, J.; Kollman, C.; Cheng, P., Closed-Loop Insulin Delivery in Suboptimally Controlled Type 1 Diabetes: A Multicentre, 12-Week Randomised Trial. *The Lancet* **2018,** *392* (10155), 1321-1329.

33. Gu, Z.; Dang, T. T.; Ma, M.; Tang, B. C.; Cheng, H.; Jiang, S.; Dong, Y.; Zhang, Y.; Anderson, D. G., Glucose-Responsive Microgels Integrated with Enzyme Nanocapsules for Closed-Loop Insulin Delivery. *ACS Nano* **2013,** *7* (8), 6758-6766.

34. Wang, J.; Ye, Y.; Yu, J.; Kahkoska, A. R.; Zhang, X.; Wang, C.; Sun, W.; Corder, R. D.; Chen, Z.; Khan, S. A., Core–Shell Microneedle Gel for Self-Regulated Insulin Delivery. *ACS Nano* **2018,** *12* (3), 2466-2473.

35. Wang, J.; Yu, J.; Zhang, Y.; Zhang, X.; Kahkoska, A. R.; Chen, G.; Wang, Z.; Sun, W.; Cai, L.; Chen, Z.; Qian, C.; Shen, Q.; Khademhosseini, A.; Buse, J. B.; Gu, Z., Charge-Switchable Polymeric Complex for Glucose-Responsive Insulin Delivery in Mice and Pigs. *Science Advances* **2019,** *5* (7), eaaw4357.

36. Zhang, Y.; Wang, J.; Yu, J.; Wen, D.; Kahkoska, A. R.; Lu, Y.; Zhang, X.; Buse, J. B.; Gu, Z., Bioresponsive Microneedles with a Sheath Structure for H2o2 and Ph Cascade-Triggered Insulin Delivery. *Small* **2018,** *14* (14), 1704181.

37. Wang, J.; Wang, Z.; Chen, G.; Wang, Y.; Ci, T.; Li, H.; Liu, X.; Zhou, D.; Kahkoska, A. R.; Zhou, Z.; Meng, H.; Buse, J. B.; Gu, Z., Injectable Biodegradable Polymeric Complex for Glucose-Responsive Insulin Delivery. *ACS Nano* **2021,** *15* (3), 4294-4304.

38. Chen, W.; Zhou, S.; Ge, L.; Wu, W.; Jiang, X., Translatable High Drug Loading Drug Delivery Systems Based on Biocompatible Polymer Nanocarriers. *Biomacromolecules* **2018,** *19* (6), 1732-1745.

39. Guo, H.; Li, H.; Gao, J.; Zhao, G.; Ling, L.; Wang, B.; Guo, Q.; Gu, Y.; Li, C., Phenylboronic Acid-Based Amphiphilic Glycopolymeric Nanocarriers for in Vivo Insulin Delivery. *Polymer Chemistry* **2016,** *7* (18), 3189-3199.

40. Yao, Y.; Zhao, L.; Yang, J.; Yang, J., Glucose-Responsive Vehicles Containing Phenylborate Ester for Controlled Insulin Release at Neutral Ph. *Biomacromolecules* **2012,** *13* (6), 1837-1844.

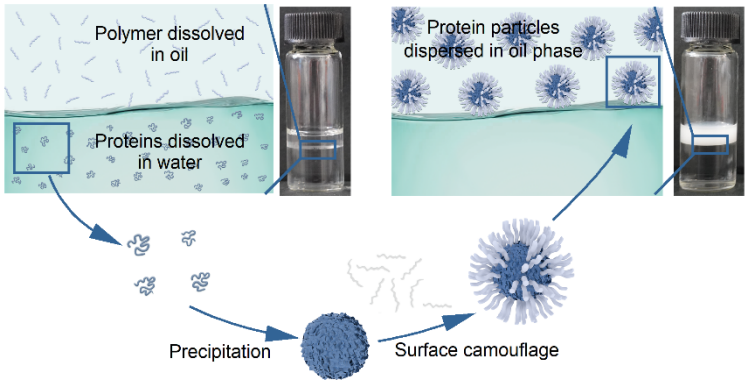
Polymer dissolved in oil
Proteins dissolved in water
Protein particles dispersed in oil phase
Precipitation
Surface camouflage

TOC graphic